THE JOURNAL OF BIOLOGICAL CHEMISTRY VOL. 282, NO. 35, pp. 25737–25747, August 31, 2007

Structural and Membrane Binding Analysis of the Phox Homology Domain of Bem1p

BASIS OF PHOSPHATIDYLINOSITOL 4-PHOSPHATE SPECIFICITY[*] [S]

Received for publication, April 4, 2007, and in revised form, May 29, 2007 Published, JBC Papers in Press, June 20, 2007, DOI 10.1074/jbc.M702861200

Robert V. Stahelin[‡§¶], **Dimitrios Karathanassis**[‖1], **Diana Murray**[**], **Roger L. Williams**[‖], **and Wonhwa Cho**[‡2]

From the [‡]*Department of Chemistry, University of Illinois, Chicago, Illinois 60607-7061, the* [§]*Department of Biochemistry and Molecular Biology, Indiana University School of Medicine, and the* [¶]*Department of Chemistry and Biochemistry and the Walther Center for Cancer Research, University of Notre Dame, South Bend, Indiana 46617, the* [‖]*Medical Research Council Laboratory of Molecular Biology, Cambridge CB2 2QH, United Kingdom, and the* [**]*Department of Microbiology and Immunology, Weill Medical College of Cornell University, New York, New York 10021*

Phox homology (PX) domains, which have been identified in a variety of proteins involved in cell signaling and membrane trafficking, have been shown to interact with phosphoinositides (PIs) with different affinities and specificities. To elucidate the structural origin of the diverse PI specificity of PX domains, we determined the crystal structure of the PX domain from Bem1p that has been reported to bind phosphatidylinositol 4-phosphate (PtdIns(4)P). We also measured the membrane binding properties of the PX domain and its mutants by surface plasmon resonance and monolayer techniques and calculated the electrostatic potentials for the PX domain in the absence and presence of bound PtdIns(4)P. The Bem1p PX domain contains a signature PI-binding site optimized for PtdIns(4)P binding and also harbors basic and hydrophobic residues on the membrane-binding surface. The membrane binding of the Bem1p PX domain is initiated by nonspecific electrostatic interactions between the cationic membrane-binding surface of the domain and anionic membrane surfaces, followed by the membrane penetration of hydrophobic residues. Unlike other PX domains, the Bem1p PX domain has high intrinsic membrane penetrating activity in the absence of PtdIns(4)P, suggesting that the partial membrane penetration may occur before specific PtdIns(4)P binding and last after the removal of PtdIns(4)P under certain conditions. This structural and functional study of the PtdIns(4)P-binding Bem1p PX domain provides new insight into the diverse PI specificities and membrane-binding mechanisms of PX domains.

Phosphoinositides (PIs),[3] phosphorylated derivatives of phosphatidylinositol (PtdIns), regulate diverse biological processes such as growth, membrane trafficking, cell survival, and cytoskeletal rearrangement (1, 2). PtdIns is reversibly phosphorylated at the D3, D4, or D5 position to yield seven different PIs, which are both transiently and constitutively present in different cell membranes. Research in the past decade has revealed that a large number of cellular proteins reversibly translocate to these specific subcellular locations to form lipid-protein interactions (3, 4). These interactions play a crucial role in cell signaling and membrane trafficking, and the PIs are responsible for regulating not only the localization but also, in many instances, the biological activity of their effector protein (2, 5, 6). Many PI effector proteins typically contain one or more modular domains specialized in PI binding (7, 8). PI-binding domains include pleckstrin homology (PH) (9, 10), Fab1/YOTB/Vac1/EEA1 (FYVE) (11, 12), Phox homology (PX) (13, 14), epsin N-terminal homology (ENTH) (15–17), AP180 N-terminal homology (ANTH) (15–17), Bin/amphiphysin/Rversus (BAR) (17–20), band 4.1/ezrin/radixin/moesin (FERM) (21), tubby (22), and protein kinase C conserved 2 (C2) (23–26) domains.

PI metabolism is also crucial to the budding yeast *Saccharomyces cerevisiae* (27), although the function and regulation of PIs and PI effectors are still less defined. Growth of *S. cerevisiae* by budding requires polarity establishment to expand the cell wall, and this bud emergence process is tightly regulated and occurs at distinct sites in new cells (28, 29) following a period of uniform growth during G_1. Recent studies have identified a number of key players in the initiation of bud formation: Cdc42p, a small GTPase protein; Cdc24p, a GDP/GTP exchange factor for Cdc42p; and Bem1p, a putative scaffold protein (30–32). Bem1p is a multidomain scaffolding protein that binds Cdc42p with its N-terminal Src homology 3 (SH3) domain (33), and this interaction is critical for proper Cdc42p activation (34). Bem1p has been shown to migrate to the plasma

* This work was supported by National Institutes of Health Grant GM68849 (to W. C.) and by the Medical Research Council (to R. L. W.). The costs of publication of this article were defrayed in part by the payment of page charges. This article must therefore be hereby marked "*advertisement*" in accordance with 18 U.S.C. Section 1734 solely to indicate this fact.

The atomic coordinates and structure factors (code 2v6v) have been deposited in the Protein Data Bank, Research Collaboratory for Structural Bioinformatics, Rutgers University, New Brunswick, NJ (http://www.rcsb.org/).

[S] The on-line version of this article (available at http://www.jbc.org) contains supplemental Fig. 1.

[1] Present address: Research Center for Biomaterials S. A., 15, 16562 Glyfalda-Athens, Greece.

[2] To whom correspondence should be addressed: Dept. of Chemistry (M/C 111), University of Illinois, 845 West Taylor St., Chicago, IL 60607-7061. Tel.: 312-996-4883; Fax: 312-996-2183; E-mail: wcho@uic.edu.

[3] The abbreviations used are: PIs, phosphoinositides; PtdIns, phosphatidylinositol; PH, pleckstrin homology; FYVE, Fab1/YOTB/Vac1/EEA1; PX, Phox homology; ENTH, epsin N-terminal homology; SH3, Src homology 3; PLD, phospholipase D; CISK, cytokine-independent survival kinase; PI3K-C2α, phosphoinositide 3-kinase C2α; PS, phosphatidylserine; SPR, surface plasmon resonance; POPC, 1-palmitoyl-2-oleoyl-*sn*-glycero-3-phosphocholine; POPS, 1-palmitoyl-2-oleoyl-*sn*-glycero-3-phosphoserine; POPE, 1-palmitoyl-2-oleoyl-*sn*-glycero-3-phosphoethanolamine; CHAPS, 3-[(3-cholamidopropyl)dimethylammonio]-1-propanesulfonic acid; MAD, multiwavelength anomalous dispersion; Bem1p-PX, Bem1p PX domain; OSBP, oxysterol-binding protein; PP_{II}, type II polyproline helix.

membrane during budding and mating, where it can serve as an adaptor for Cdc42p and other proteins (35, 36). The mechanism behind the plasma membrane translocation of Bem1p is still unknown. Interestingly, Bem1p has been shown to harbor a PX domain that binds PtdIns(4)P (37). PtdIns(4)P has been shown to be localized to both the plasma membrane and secretory machinery in yeast (27). The molecular details of a number of protein-protein interactions have been mapped out for Bem1p (38), but much less is known about its lipid binding properties, in particular the role of its PX domain in the membrane recruitment of Bem1p.

The PX domain is a structural module composed of 100–140 amino acids that was first identified in the $p40^{phox}$ and $p47^{phox}$ subunits of NADPH oxidase (39) and has since been found in a variety of other proteins involved in membrane trafficking (*e.g.* Mvp1p, Vps5p, Bem1p, Grd19p, and the sorting nexin family of proteins) and cell signaling (*e.g.* phospholipase D (PLD), PI 3-kinases, cytokine-independent survival kinase (CISK), and five SH3 domains (FISH)). Sequence comparisons of PX domains have shown that they contain several conserved regions, including a proline-rich stretch (P*XX*P) and a number of basic residues (13, 14). Subsequently, PX domains have been shown to interact with different PIs via conserved basic residues and to target the host proteins to specific subcellular locations (40–45). PX domains are similar to the PH domain in that they exhibit broad PI specificity. It was initially reported that PX domains of Vam7p (41), sorting nexin-3 (44), and $p40^{phox}$ (40) specifically interact with PtdIns(3)P *in vitro* and also target the host proteins to early endosomes in the cell. It was also reported that most of the yeast PX domains bind PtdIns(3)P (45), albeit with varying affinities. On the hand other, the PX domain of Class II PI 3-kinase C2α (PI3K-C2α) interacts with PtdIns(4,5)P_2 (43, 46), whereas the $p47^{phox}$ PX domain preferentially interacts with PtdIns(3,4)P_2 (47). Also, the PX domain of the yeast protein PLD1 has specificity for PtdIns(3,4,5)P_3 (48, 49), whereas the PX domain of NOXO1 (Nox-organizing protein-1) was reported to bind PtdIns(4)P, PtdIns(5)P, and PtdIns(3,5)P_2 (50).

Recent structural and modeling studies of a variety of PX domains have lead to a better understanding of the mechanisms of stereospecific PI recognition and membrane binding by PX domains. Earlier structural studies focused on PX domains that interact with PtdIns(3)P. For example, the crystal structure of the $p40^{phox}$-PtdIns(3)P complex illustrated how the domain achieves the stereospecific recognition of PtdIns(3)P (51). The structure revealed that basic residues Lys^{92} and Arg^{58} specifically form hydrogen bonds with the D1- and D3-phosphates of PtdIns(3)P, respectively. The crystal structure of the CISK PX domain showed that this domain also has all the basic residues necessary for binding the D3-phosphate of PtdIns(3)P (52). The crystal structures of the free and PtdIns(3)P-bound PX domains of the yeast Grd19p protein showed the lipid-induced local conformational changes in the membrane-binding loop (53). NMR studies of the Vam7p PX domain have also elucidated the origin of its PtdIns(3)P specificity and the membrane-docking mechanism (54, 55).

In addition to these studies on PtdIns(3)P-binding PX domains, structural studies on the $p47^{phox}$ (47) and PI3K-C2α (46) PX domains that specifically interact with PtdIns(3,4)P_2 and PtdIns(4,5)P_2, respectively, showed how these PX domains achieve different PI specificities. In particular, the crystal structure of the PX domain of $p47^{phox}$ revealed that this PX domain has a smaller secondary pocket that binds phosphatidic acid or phosphatidylserine (PS) (47). A modeling study of the PLD1 PX domain also suggested that it has two binding pockets, a primary site specific for PtdIns(3,4,5)P_3 and a second site that interacts nonspecifically with anionic phospholipids (49).

To date, no structural information is available for the PX domains with specificity for PtdIns(4)P. To gain a better understanding of differential PI recognition and membrane-binding mechanisms of PX domains, we determined the x-ray crystal structure of the Bem1p PX domain, which has been reported to bind PtdIns(4)P (37). We also measured the interaction of this domain and mutations with model membranes containing various PIs by surface plasmon resonance (SPR) and monolayer penetration analyses and calculated the electrostatic potential of the domain in the absence and presence of lipid ligand. The results provide new insight into how the Bem1p PX domain specifically recognizes PtdIns(4)P and how the domain may be targeted to the PtdIns(4)P-containing membranes.

EXPERIMENTAL PROCEDURES

Materials—1-Palmitoyl-2-oleoyl-*sn*-glycero-3-phosphatidic acid, 1-palmitoyl-2-oleoyl-*sn*-glycero-3-phosphocholine (POPC), 1-palmitoyl-2-oleoyl-*sn*-glycero-3-phosphoserine (POPS), and 1-palmitoyl-2-oleoyl-*sn*-glycero-3-phosphoethanolamine (POPE) were from Avanti Polar Lipids (Alabaster, AL). PtdIns(3)P, PtdIns(4)P, PtdIns(5)P, PtdIns(3,4)P_2, PtdIns(3,5)P_2, PtdIns(4,5)P_2, and PtdIns(3,4,5)P_3 were purchased from Cayman (Ann Arbor, MI). Phospholipid concentrations were determined by phosphate analysis (56). The LiposoFast microextruder and 100-nm polycarbonate filters were from Avestin (Ottawa, Ontario, Canada). Fatty acid-free bovine serum albumin was from Bayer (Kankakee, IL). Restriction endonucleases and other enzymes for molecular biology were from New England Biolabs (Beverly, MA). CHAPS and octyl glucoside were from Sigma and Fisher, respectively. The Pioneer L1 sensor chip was from Biacore (Piscataway, NJ).

Structure Determination—For structure determination, DNA encoding the yeast Bem1p PX domain (residues 266–413) was amplified by PCR from yeast genomic DNA and subsequently cloned with a C-terminal His_6 affinity tag in the pJL vector. The protein was expressed in the methionine-requiring auxotrophic *Escherichia coli* strain 834(DE3) and purified by Ni^{2+} affinity, heparin, and gel filtration chromatography. The protein in gel filtration buffer (20 mM Tris-HCl (pH 7.4 at 25 °C), 100 mM NaCl, and 5 mM dithiothreitol) was concentrated to 5 mg/ml. Crystals were obtained in sitting drops (3 μl of protein plus 3 μl of reservoir solution) that were incubated at 14 °C over a reservoir consisting of 0.2 M NaCl, 0.1 M sodium/potassium phosphate (pH 6.2), 10% polyethylene glycol 8000, and 2 mM dithiothreitol. Crystals were visible after 12 h and grew to full size within 1 week.

For diffraction data collection, crystals were cryoprotected by adding Paratone-N to the drop and removing excess mother liquor surrounding the crystal. Loops containing the crystal in

TABLE 1
Data collection, structure determination, and refinement statistics

	Peak[a]	Inflection[a]	Remote[a]
Data collection statistics			
Resolution (Å)	1.7	1.7	1.5
Completeness (last shell)	88 (51)	88 (51)	99.6 (99.4)
R_{merge} (last shell)[b]	0.049 (0.30)	0.049 (0.29)	0.068 (0.38)
Multiplicity (last shell)	3.4 (2.5)	3.4 (2.5)	3.5 (3.6)
$\langle I/\sigma \rangle$ (last shell)	18.2 (2.5)	17.7 (2.1)	8.9 (1.5)
Unit cell ($P2_12_12_1$)	$a = 61.0, b = 71.6, c = 75.3$		
Phasing statistics[a]			
Isomorphous phasing power[c]	0.5		1.3
Anomalous phasing power[c]	1.4	0.9	1.0
Se sites found	4		
FOM[d] after SHARP	0.32		
FOM after SOLOMON	0.78		
FOM after DM	0.92		
Refinement statistics[a]			
Resolution range (Å)	51.9–1.5		
Number of reflections	50,498		
Cutoff (F/σ)	None		
Completeness (%)	99.4		
Protein atoms	4339		
Average total B factor (Wilson B factor; Å^2)	16 (19)		
Waters	9		
R_{cryst}[e]	0.22		
R_{free} (% data used)[e]	0.25 (5.1)		
r.m.s.d. from ideality[f]			
Bonds (Å)	0.012		
Angles	1.2°		
Dihedrals	4.9°		

[a] Data sets were collected at European Synchrotron Radiation Facility beamline ID14-4 at $\lambda = 0.9793$, 0.9796, and 0.9393 Å for peak, inflection, and remote, respectively, using an ADSC detector. The MAD phase refinement was carried out at 1.7-Å resolution. The remote data set was used for the structure refinement. The MAD phasing was carried out using inflection, peak, and remote data sets.
[b] $R_{merge} = \Sigma_{hkl}\Sigma_i|I_i(hkl) - \langle I(hkl)\rangle|/\Sigma_{hkl}\Sigma_i I_i(hkl)$.
[c] Values are the ratio of the heavy atom structure factor amplitudes to the lack-of-closure error.
[d] FOM, figure of merit.
[e] R_{cryst} and $R_{free} = \Sigma||F_o| - |F_c||/\Sigma|F_o|$. R_{free} was calculated with the percentage of the data shown in parentheses.
[f] Root mean square deviations are for bond angles and lengths with regard to the parameters of Engh and Huber (89).

Paratone-N with minimal mother liquor were flash-frozen in a nitrogen stream at 100 K. A three-wavelength multiwavelength anomalous dispersion (MAD) data collection was carried out. Table 1 summarizes the data collection statistics. Images were processed with the program MOSFLM (57) and refined with SCALA (58). Four selenium sites were located with SOLVE (59) and refined with SHARP (60). After density modification with SOLOMON (61) and DM (62), an initial model was automatically built using ARP/wARP (63) and manually adjusted using program O (64). The model was refined with REFMAC (65). There are two molecules in the asymmetric unit. Residues 266–275 and 411–413 are not ordered in the electron density map. Ramachandran analysis with the program PROCHECK (66) showed 92% of residues in the most probable regions and no residues in the disallowed area. The refinement statistics are given in Table 1. A representative section of the experimental and refined electron densities is illustrated in supplemental Fig. 1.

Mutagenesis and Protein Expression—Mutagenesis of the Bem1p PX domain (Bem1p-PX) was performed using the overlap extension PCR method (67). Constructs were subcloned into the pET21a vector containing a C-terminal His_6 tag and transformed into DH5α cells for plasmid isolation. After checking each construct for correct sequence by DNA sequencing, the plasmid was transformed into BL21(DE3) cells for protein expression. The PX domains for biophysical studies were expressed and purified as described previously (46). The oxysterol-binding protein (OSBP) PH domain was expressed in the same manner and purified by Ni^{2+} affinity chromatography. The PH domain of PtdIns(4)P adaptor protein-1 (FAPP1) was expressed and purified as a glutathione *S*-transferase fusion protein as described previously (68). Protein concentration was then determined by the BCA method (Pierce).

Monolayer Measurements—Penetration of the Bem1p PX domain as well as the FAPP1 and OSBP PH domains into the lipid monolayers of different compositions was measured in terms of the change in surface pressure (π) at constant surface area using a 10-ml circular Teflon trough and Wilhelmy plate connected to a Cahn microbalance as described previously (69). Once the initial surface pressure reading (π_0) of monolayer spread onto the subphase (10 mm HEPES containing 0.16 m KCl (pH 7.4)) had been stabilized (after ~5 min), the protein solution was injected into the subphase through a small hole drilled at an angle through the wall of the trough, and the change in surface pressure ($\Delta\pi$) was measured as a function of time. The maximal $\Delta\pi$ value at a given π_0 depended on the protein concentration, and thus, protein concentrations in the subphase were maintained high enough to ensure that the observed $\Delta\pi$ represented a maximal value. The critical surface pressure (π_c) was determined by extrapolating the $\Delta\pi$ *versus* π_0 plot to the x axis.

SPR Measurements—All SPR measurements were performed at 23 °C in 10 mM HEPES (pH 7.4) containing 0.16 M KCl as described previously (68, 70, 71). Following washing of the sensor chip surfaces, POPC/POPE/PI (77:20:3) and POPC/POPE (80:20) vesicles were injected at 5 ml/min onto the active surface and the control surface, respectively, to give the same resonance unit (RU) values. The level of lipid coating for both surfaces was kept at the minimum that is necessary for preventing nonspecific adsorption to the sensor chips. This low surface coverage minimized the mass transport effect and kept the total protein concentration (P_0) above the total concentration of protein-binding sites on vesicles (72). Under our experimental conditions, no binding to the control surface was detected beyond the refractive index change for all proteins. Each lipid layer was washed three times with 10 ml of 50 mM NaOH at 100 ml/min. Typically, no decrease in lipid signal was seen after the first injection. Equilibrium SPR measurements were done at the flow rate of 2 ml/min to allow sufficient time for the R values of the association phase to reach near-equilibrium values (R_{eq}) (46). After sensorgrams were obtained for five or more different concentrations of each protein within a 10-fold range of K_d, each of the sensorgrams was corrected for refractive index change by subtracting the control surface response from it. Assuming a Langmuir-type binding between the protein (P) and protein-binding sites (M) on vesicles (*i.e.* P + M ↔ PM) (72), R_{eq} values were then plotted *versus* P_0, and the K_d value was determined by a nonlinear least-squares analysis of the binding isotherm using the following equation: $R_{eq} = R_{max}/(1 + K_d/P_0)$ (72). Each data set was repeated three or more times to calculate the means ± S.D.

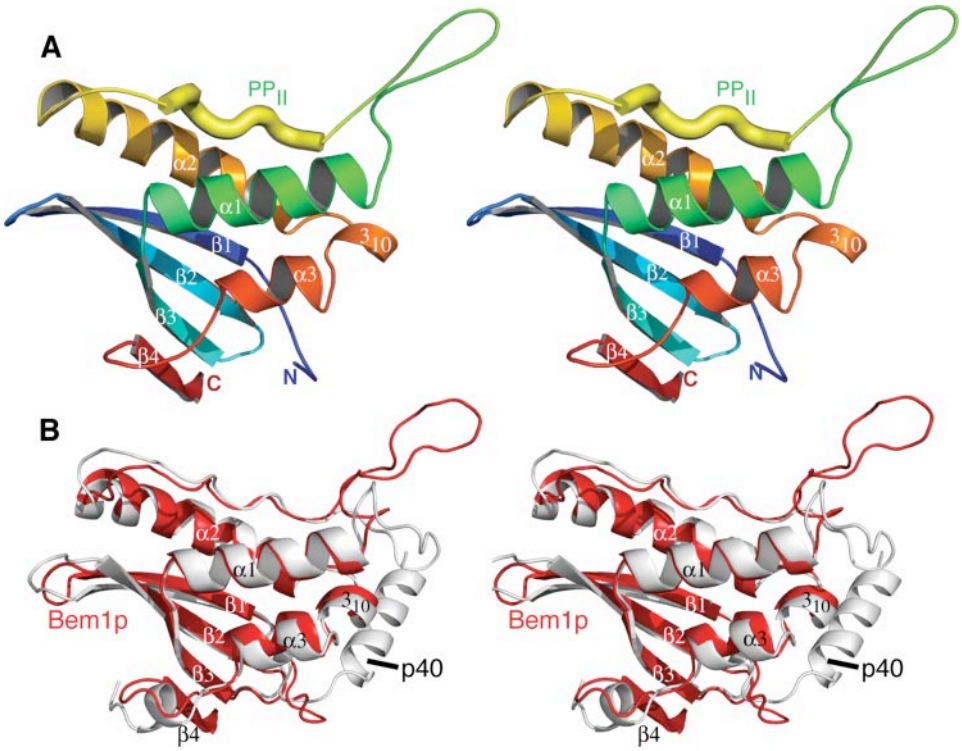

FIGURE 1. **Bem1p PX domain overall structure.** *A*, the Bem1p PX domain is depicted in stereo as a ribbon representation colored rainbow from the N to the C terminus. *B*, shown is a stereo diagram of the ribbon diagram of Bem1p-PX (*red*) overlaid with the ribbon diagram of p40^{phox}-PX (*white*).

Molecular Modeling and Electrostatic Potential Calculations—The electrostatic properties of the Bem1p PX domain with and without bound lipid were calculated with a modified version of the program Delphi and visualized in the program GRASP (73) as described previously (74). The electrostatic calculations performed used partial charges taken from the CHARMM27 force field (75) and spatial coordinates from the structure of the Bem1p PX domain. Inositol 1,4-bisphosphate was docked onto Bem1p using superposition of the p40^{phox} PX domain (Protein Data Bank code 1H6H) (51) with Bem1p and copying the coordinates of Bem1p from the superposition and those of the ligand from 1H6H. Steric clashes were fixed by side chain minimization calculation with MODELLER (76).

RESULTS

Description of the Overall Structure—Recent structural studies have elucidated the basis of the PI specificity of several PX domains, including the PtdIns(3)P-binding p40^{phox} (51), Grd19p (53), and Vam7p (54, 55) PX domains; the PtdIns(3,4)P_2-coordinating p47^{phox} PX domain (47); the PtdIns(3,4,5)P_3-binding CISK PX domain (77); and the PtdIns(4,5)P_2-binding PI3K-C2α PX domain (46). To understand the mechanism by which small and structurally similar PX domains achieve such diverse PI specificity, we determined by x-ray diffraction analysis the crystal structure of the Bem1p PX domain (PDB ID: 2v6v) that has unique specificity for PtdIns(4)P (37).

The Bem1p PX domain crystallized in space group $P2_12_12_1$ with two molecules in the asymmetric unit. The crystals diffracted to 1.5-Å resolution, and the structure was determined using MAD phasing for a selenomethionine-substituted protein. The two molecules in the asymmetric unit are nearly identical. The Bem1p PX domain features the common PX domain fold consisting of a three-stranded meander topology β-sheet packed against a helical subdomain, which contains three α-helices, a type II polyproline helix (PP_{II}), and a 3_{10} helix (Fig. 1*A*). The largest differences in the fold with respect to other PX domains are in the N- and C-terminal extensions and in the α1-PP_{II} loop (Fig. 1*B*). The Bem1p PX domain has a fourth short β-strand (β4) at its C terminus. The α1-PP_{II} loop is a region that is variable among the PX domains.

The most striking difference between a PtdIns(3)P-binding PX domain and the Bem1p PX domain is that a basic residue critical for the D3-phosphate interaction in PtdIns(3)P binders (*e.g.* Arg^{58} in p40^{phox}-PX) is replaced by Tyr^{317} in Bem1p. The structure of the Bem1p PX domain reveals that Tyr^{317} is actually pointing in the opposite direction of the pocket itself (Fig. 2, *A* and *C*), leaving much of the space occupied by the side chain of Arg^{58} in p40^{phox} empty (Fig. 2*D*). Only the rotamer of Tyr^{317} pointing away could provide sufficient volume to the pocket for PI binding. Another important determinant of PtdIns(3)P binding is Lys^{92} in p40^{phox}-PX, which interacts with the D1-phosphate of PtdIns(3)P, along with Arg^{60}, and helps orient the lipid in the correct position relative to the pocket (Fig. 2*D*). This interaction is absent in Bem1p, as the position corresponding to Lys^{92} in p40^{phox}-PX is occupied by the buried Pro^{357} (Fig. 2, *A* and *C*).

The Bem1p-PX Tyr^{318} side chain and its analogs in the other PX domains mark the floor of the lipid-binding pocket (Fig. 2*C*), under which a hydrophobic core is conserved throughout the PX domains. Besides Tyr^{318}, this core is made up of the conserved residues Phe^{300}, Phe^{321}, and Leu^{373}. Bem1p-PX Tyr^{318} clearly superimposes with p40^{phox}-PX Tyr^{59} (Fig. 2*D*), but in contrast to p40^{phox}-PX, this residue cannot contribute to inositol ring stacking interactions, as it is sheltered by the Pro^{357} side chain (Fig. 2*C*). This is reminiscent of p47^{phox}-PX, in which, again, a completely buried Pro^{78} prohibits access to the aromatic ring.

In addition to other conserved lipid-binding determinants, the loop spanning PP_{II} and helix α2, which is the region with least sequence similarity among PX domains, seems to be instrumental in the lipid binding selectivity of PX domains. In the Bem1p PX domain, two features of this variable loop prevent PIs from binding in an orientation similar to that seen for PtdIns(3)P-binding p40^{phox} and Vam7p PX domains. The position equivalent to Tyr^{94} in p40^{phox}-PX, which is responsible for hydrophobic contacts with the diacylglycerol moiety of

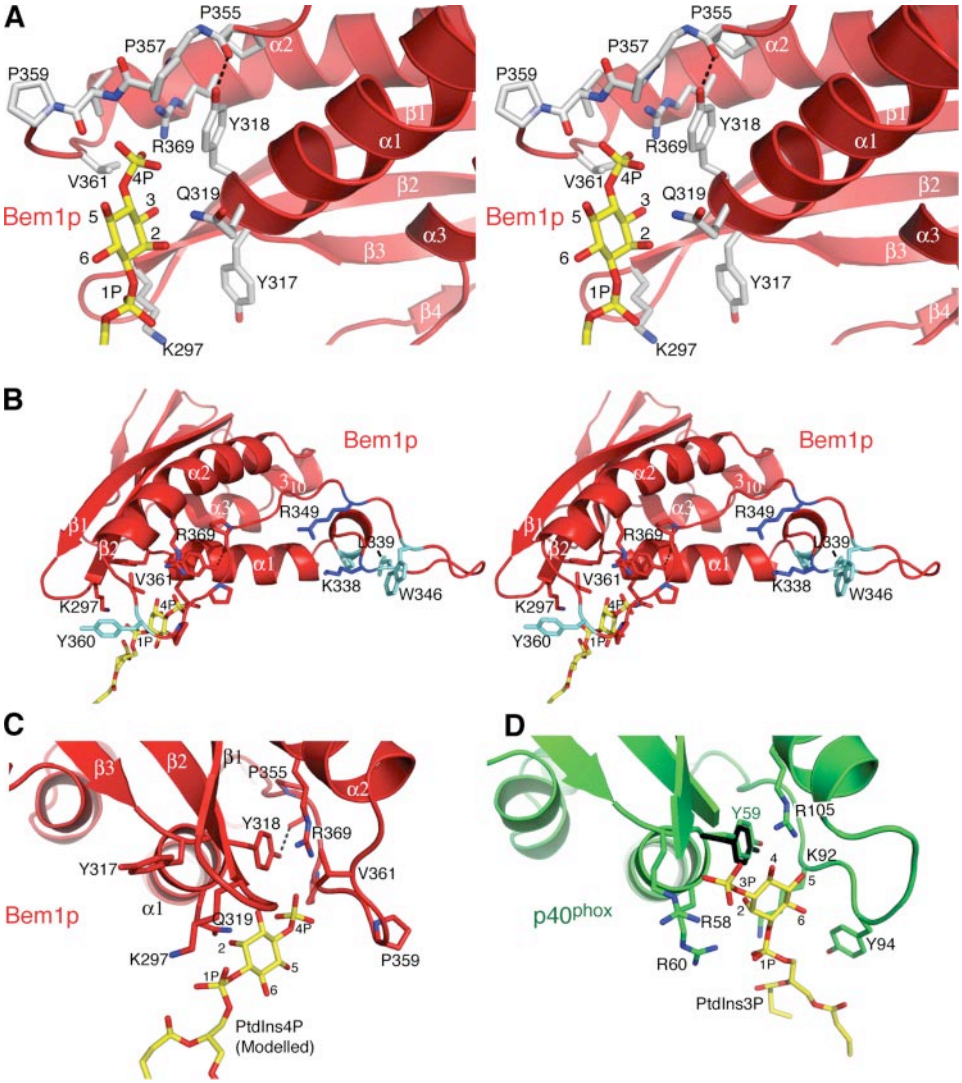

FIGURE 2. **PI-binding pocket of the Bem1p PX domain.** *A*, stereo view of the PtdIns(4)P-binding pocket. A model of PtdIns(4)P has been placed in the pocket to reflect our view of possible PtdIns(4)P binding. No changes have been introduced in the pocket itself to accommodate PtdIns(4)P. *B*, stereo view of the overall Bem1p PX domain illustrating the PtdIns(4)P-binding site and the secondary cationic site. Basic residues in the secondary site are shown as *blue sticks*. Hydrophobic residues that may be involved in membrane penetration are shown as *aquamarine sticks*. *C* and *D*, Bem1p-PX with modeled PtdIns(4)P and p40^{phox}-PX with bound PtdIns(3)P (Protein Data Bank code 1H6H) shown in the same orientation. In *D*, Tyr^{318} in Bem1p-PX (*black sticks*) is superimposed on Tyr^{59} in p40^{phox}-PX.

PtdIns(3,4)P_2 with the D2-OH pointing down or PtdIns(4,5)P_2 with the D2-OH pointing up or down, because either possibility would position a phosphate adjacent to Tyr^{318} that cannot effectively neutralize negative charges. The possibility of PtdIns(5)P binding the pocket in a similar orientation to the one suggested for PtdIns(4)P is unlikely, as it would disrupt hydrogen bonds with the inositol ring and the D1-phosphate.

Two residues in Bem1p that remain in positions closely related to their equivalents in p40^{phox}-PX are Arg^{369} in helix α2, which superimposes with Arg^{105} of p40^{phox}-PX, and Gln^{319}, which replaces Arg^{60} of p40^{phox}-PX with its shorter side chain tilted more toward helix α1 (Fig. 2, *C* and *D*). Arg^{105} in p40^{phox}-PX is responsible for interaction with the D4-OH in PtdIns(3)P. In our model of PtdIns(4)P bound to Bem1p (Fig. 2*C*), its Bem1p equivalent, Arg^{369}, is mediating interaction with the D4-phosphate of PI. With PtdIns(4)P placed in this orientation, the D4-phosphate would form hydrogen bonds with Arg^{369} and the backbone amide of Val^{358} at the start of the loop following PP_{II}. With the inositol ring positioned at a "slant" relative to the pocket, our model of PtdIns(4)P steers clear of Val^{361} while permitting the N-ϵ2 of Gln^{319} to form a hydrogen bond with the D2-OH group of the inositol moiety. An interaction with the D2-OH has not been observed previously for PX domains. Additionally, this orientation could permit the N-ϵ of the Lys^{297} side chain to assume a role of stabilizing the D1-phosphate, as seen with Lys^{92} in p40^{phox}-PX. Lys^{297} is not conserved among the PX domains. Instead, this position is usually occupied by a valine. The Vam7p PX domain has Lys^{25} in this position, but the side chain of this lysine points away from the lipid-binding pocket. In one of the two Bem1p molecules in the asymmetric unit, part of the side chain of Lys^{297} is disordered, suggesting flexibility.

In general, the membrane-binding surfaces of PI- or other lipid-binding proteins contain basic and hydrophobic residues, which are involved in initial membrane adsorption and membrane penetration, respectively (7). In the case of PX domains, clustered basic residues are often found in the α1-PP_{II} loop (7). Also, hydrophobic residues are present in the PP_{II}-α2 loop of most PX domains (7) and also in the α1-PP_{II} loop of some PX

PtdIns(3)P (Fig. 2*D*), is occupied in Bem1p by an exposed Pro^{359} (Fig. 2*C*), which precludes the possibility of interactions with the diacylglycerol moiety in a p40^{phox}-like manner. Additionally, the backbone of the loop leading into helix α2 forms an accented curve between residues 360 and 362, which forces Val^{361} to sway inwards into the pocket (Fig. 2, *A*–*C*). Compared with the extended conformation of the analogous region in p40^{phox}-PX, the specific turn in Bem1p is much tighter, and the Val^{361} side chain is sufficiently bulky to make the site too cramped for lipids to fit. To model plausible binding modes, it is essential to consider both orientations of the inositol ring in which the axial 2-OH points down toward the floor of the binding pocket (as it does for p40^{phox}-PX) and orientations with the inositol ring flipped 180° around the C1-C4 axis. In our proposed orientation of PtdIns(4)P (Fig. 2), Val^{361} would prevent access to doubly phosphorylated PIs, *i.e.*

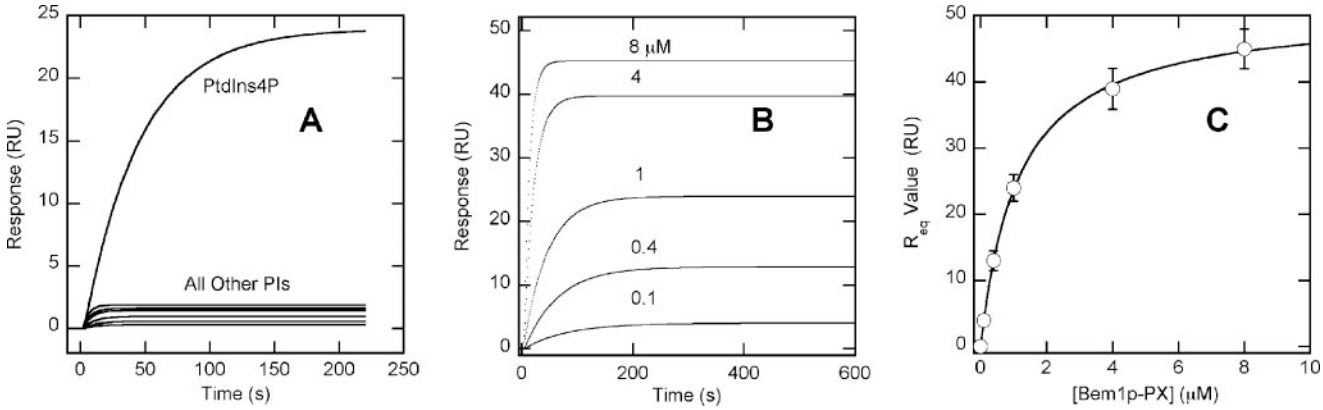

FIGURE 3. **Equilibrium SPR binding analysis of the Bem1p PX domain.** *A*, the Bem1p PX domain (1 μM) was injected over a POPC/POPE/PI (77:20:3) surface to gauge the affinity and specificity for different PIs, including PtdIns(3)P, PtdIns(4)P, PtdIns(5)P, PtdIns(3,4)P_2, PtdIns(3,5)P_2, PtdIns(4,5)P_2, and PtdIns(3,4,5)P_3. The SPR response curves for respective PIs are shown after background correction for binding to the control surface coated with POPC/POPE (80:20). Binding to the control surface was minimal, and little evidence of nonspecific binding was evident at 1 μM protein. *B*, the Bem1p PX domain was injected at 2 μl/min at varying concentrations (0.1, 0.4, 1, 4, and 8 μM from bottom to top) over the POPC/POPE/PtdIns(4)P (77:20:3) surface, and R_{eq} values were measured. *C*, a binding isotherm was generated from the R_{eq} ($n = 3$) *versus* concentration of Bem1p-PX plot. The *solid line* represents a theoretical curve constructed from R_{max} (51 $\pm$ 0.5) and K_d (1.2 $\pm$ 0.1 μM) values determined by nonlinear least-squares analysis of the isotherm using $R_{eq} = R_{max}/(1 + K_d/P_0)$. 10 mM HEPES (pH 7.4) containing 0.16 M KCl was used for all measurements. *RU*, resonance units.

domains, such as p47^{phox}-PX (47, 78). The crystal structure of Bem1p-PX shows the presence of two basic residues, Lys^{338} and Arg^{349}, in the α1-PP_{II} loop (Fig. 2*B*), which may either form a secondary lipid pocket, as seen with p47^{phox}-PX (47) and PLD1-PX (49), or interact nonspecifically with anionic phospholipids. Also, both the PP_{II}-α2 and α1-PP_{II} loops of Bem1p-PX contain exposed hydrophobic residues (*i.e.* Tyr^{360} in the PP_{II}-α2 loop and Trp^{346} in the α1-PP_{II} loop) (Fig. 2*B*), suggesting that both loops are involved in membrane penetration.

Membrane Binding of Bem1p-PX—To determine the functional roles of the putative phospholipid-binding residues in Bem1p-PX, we measured the vesicle binding of wild-type Bem1p-PX and a series of site-specific mutants by SPR and monolayer penetration analyses. We first measured the PI specificity of the Bem1p PX domain by SPR analysis. In these experiments, an active surface was coated with POPC/POPE/PI (77:20:3), whereas a control surface was coated with POPC/POPE (80:20). Initial screening was performed with the injection of 1 μM Bem1p-PX into the sensor coated with various PI-containing vesicles (Fig. 3*A*). Clearly, the Bem1p PX domain has specificity for PtdIns(4)P, as it exhibited no detectable binding to other PI-containing vesicles. Fig. 3*B* shows representative sensorgrams for Bem1p-PX-POPC/POPE/PtdIns(4)P (77:20:3) vesicle binding, and Fig. 3*C* illustrates the binding isotherm from the sensorgrams. The K_d values determined for Bem1p-PX and its mutants are listed in Table 2.

Although the Bem1p PX domain was highly specific for PtdIns(4)P, it had modest affinity (K_d = 1.2 μM) for POPC/POPE/PtdIns(4)P (77:20:3) vesicles. Other PX domains, including p40^{phox}-PX, p47^{phox}-PX, and PI3K-C2α-PX, were shown to have >10-fold higher affinities for POPC/POPE/PI (77:20:3) vesicles containing their cognate PI molecules under similar conditions (46, 78). Because the Bem1p PX domain has a cationic patch on its putative membrane-binding surface, it was expected to have higher affinity for vesicles with higher anionic lipid contents. Indeed, the affinity of Bem1p-PX gradually increased as the POPS concentration in POPC/POPE/POPS/PtdIns(4)P (77-*X*:20:*X*:3) vesicles increased (data not shown): the Bem1p PX domain bound POPC/POPE/POPS/PtdIns(4)P (57:20:20:3) vesicles ~8-fold more tightly than POPC/POPE/PtdIns(4)P (77:20:3) vesicles (see Table 2, third column). The addition of 1-palmitoyl-2-oleoyl-*sn*-glycero-3-phosphatidic acid up to 20 mol % had the same effect (data not shown), indicating that anionic phospholipids enhance binding through nonspecific electrostatic interactions. To determine whether the membrane affinity of Bem1p-PX is comparable with that of other known PtdIns(4)P-binding domains, we also measured the membrane binding of the PH domains of OSBP (79) and FAPP1 (80) that were reported to interact with PtdIns(4)P and PtdIns(4,5)P_2. As indicated in Table 2, both PH domains had modest selectivity for PtdIns(4)P over PtdIns(4,5)P_2 (see the second and fourth columns). As far as the affinity for PtdIns(4)P-containing vesicles is concerned, these PH domains had only 2–4-fold higher affinity for POPC/POPE/POPS/PtdIns(4)P (57:20:20:3) vesicles compared with Bem1p-PX (Table 2). Collectively, these results establish that the Bem1p PX domain is the genuine PtdIns(4)P-specific domain, with overall membrane affinity comparable with other reported PtdIns(4)P-binding domains.

TABLE 2

Membrane binding properties of the Bem1p PX domain and mutants

All binding measurements were performed in 10 mM HEPES (pH 7.4) containing 0.16 M KCl ($n = 3$).

Protein	K_d for POPC/POPE/PtdIns4P (77:20:3)	K_d for POPC/POPE/POPS/PtdIns4P (57:20:20:3)	K_d for POPC/POPE/PtdIns(4,5)P_2 (77:20:3)
	μM	μM	μM
Bem1p-PX	1.2 $\pm$ 0.1	0.15 $\pm$ 0.02	ND[a]
K297A	6.0 $\pm$ 0.4	0.49 $\pm$ 0.06	NM
K338A	1.5 $\pm$ 0.3	0.43 $\pm$ 0.04	NM
W346A	4.6 $\pm$ 0.4	NM	NM
R349A	2.0 $\pm$ 0.3	0.54 $\pm$ 0.04	NM
K338A/R349A	3.5 $\pm$ 0.6	1.7 $\pm$ 0.6	NM
Y360A	9.4 $\pm$ 0.5	NM	NM
R369A	ND	>15	NM
OSBP-PH	0.1 $\pm$ 0.02	0.040 $\pm$ 0.008	0.18 $\pm$ 0.02
FAPP1-PH	0.23 $\pm$ 0.03	0.080 $\pm$ 0.002	0.4 $\pm$ 0.03

[a] ND, not detectable; NM, not measured.

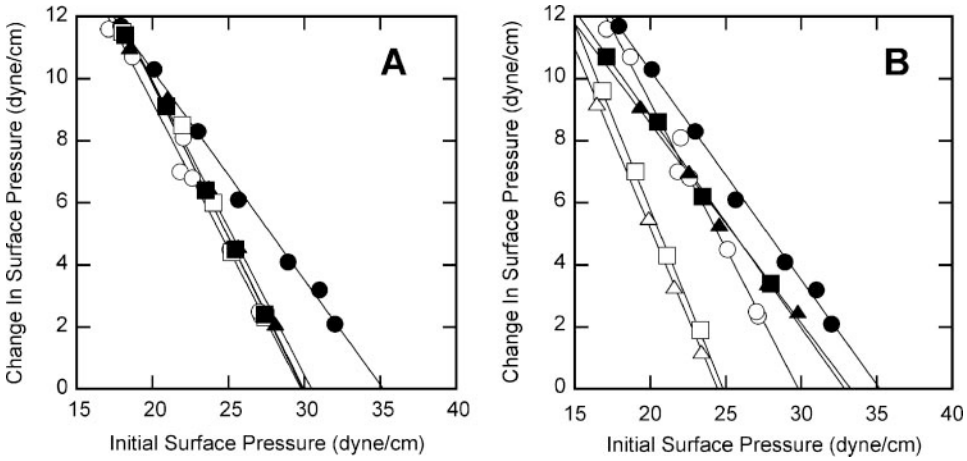

FIGURE 4. **Monolayer penetration of the Bem1p PX and OSBP and FAPP1 PH domains into various phospholipids.** *A*, $\Delta\pi$ was measured as a function of π_0 for wild-type Bem1p-PX with POPC/POPE (80:20) (○), POPC/POPE/PtdIns(4)P (77:20:3) (●), POPC/POPE/PtdIns(3)P (77:20:3) (■), POPC/POPE/PtdIns(5)P (77:20:3) (▲), and POPC/POPE/POPS (60:20:20) (□) monolayers. *B*, Bem1p (○), OSBP (□), and FAPP1 (△) were allowed interact with the POPC/POPE (80:20) monolayer, or Bem1p (●), OSBP (■), and FAPP1 (▲) were added to the POPC/POPE/PtdIns(4)P (77:20:3) monolayer. The subphase consisted of 10 mM HEPES (pH 7.4) containing 0.16 M KCl. $n = 2$.

We then measured the membrane binding of Bem1p-PX mutants to vesicles with different compositions (Table 2). In agreement with our structural analysis, mutation of a conserved Arg residue (*i.e.* R369A) abolished binding to POPC/POPE/PtdIns(4)P (77:20:3) vesicles, corroborating the notion that Arg^{369} is essential for binding to the D4-phosphate. Mutation of another cationic residue in the PtdIns(4)P-binding pocket of Bem1p-PX (K297A) had a smaller but significant effect (*i.e.* 5-fold decrease) on binding to the same vesicles, supporting the notion that this residue is also involved in PtdIns(4)P binding, presumably through coordinating the D1-phosphate.

We also determined the roles of two cationic residues in the α1-PP_{II} loop of the Bem1p PX domain (Table 2). In contrast to mutation of Arg^{369} in the PI-binding pocket, mutation of Lys^{338} or Arg^{349} had little effect on the binding of Bem1p-PX to POPC/POPE/PtdIns(4)P (77:20:3) vesicles, indicating that PtdIns(4)P does not interact with this site. However, K338A and R349A showed 3- and 4-fold reduced affinity, respectively, for more anionic POPC/POPE/POPS/PtdIns(4)P (57:20:20:3) vesicles. Also, the double mutant K338A/R349A had 11-fold lower affinity compared with the wild type for POPC/POPE/POPS/PtdIns(4)P (57:20:20:3) vesicles. Furthermore this mutant exhibited only a 2-fold difference in affinity between POPC/POPE/PtdIns(4)P (77:20:3) and POPC/POPE/POPS/PtdIns(4)P (57:20:20:3) vesicles, indicating that Lys^{338} and Arg^{349} play a significant role in nonspecific electrostatic interaction with anionic phospholipids.

Finally, we measured the effects of mutating hydrophobic residues in the PP_{II}-α2 (Tyr^{360}) and α1-PP_{II} loops (Trp^{346}) on the membrane binding of Bem1p-PX to see if they are involved in membrane penetration. Y360A exhibited 8-fold lower membrane affinity compared with the wild type for POPC/POPE/PtdIns(4)P (77:20:3) vesicles, whereas W346A showed 4-fold lower affinity compared with the wild type for the same vesicles. Thus, hydrophobic residues adjacent to the PI-binding pocket (*i.e.* PP_{II}-α2 loop) and in the α1-PP_{II} loop play a significant role in membrane binding and may be involved in membrane penetration.

Membrane Penetration of Bem1p-PX—Recent studies have shown that PIs can specifically induce the membrane penetration of the FYVE (68), PX (46, 49, 54, 78), and ENTH (81) domains. To determine whether or not PtdIns(4)P can also elicit the membrane penetration of Bem1p-PX, we first measured the penetration of the PX domain into monolayers with different lipid compositions (Fig. 4*A*). Interestingly, the Bem1p PX domain was able to penetrate the POPC/POPE (80:20) monolayer with surface pressure up to 30 dynes/cm. PI-independent membrane penetration has been reported for a few domains, including the PH domain of phospholipase Cδ1 (82) and $p47^{phox}$-PX (78). However, this type of strong PI-independent monolayer penetrating activity has not been seen with any PI-binding domains that typically cannot penetrate the monolayer with surface pressure above 25 dynes/cm in the absence of their cognate PI molecules (46, 49, 78). Because the surface pressure of cell membranes has been estimated to be 31–35 dynes/cm (83–85), this also implies that Bem1p-PX may be able to partially penetrate cell membranes even in the absence of PtdIns(4)P under certain conditions.

Although Bem1p-PX had high intrinsic monolayer penetrating power, incorporation of 3 mol % PtdIns(4)P into the monolayer (*i.e.* POPC/POPE/PtdIns(4)P (77:20:3)) further increased its monolayer penetration, allowing it to penetrate the monolayer with surface pressure up to 35 dynes/cm (Fig. 4*A*). This increase was a PtdIns(4)P-specific effect because 3 mol % PtdIns(3)P, PtdIns(5)P, or POPS in the monolayer did not have detectable effects. We also measured the effect of PtdIns(4)P on the monolayer penetration of the PH domains of OSBP and FAPP1 (Fig. 4*B*). Both OSBP and FAPP1 PH domains displayed much lower monolayer penetration than Bem1p-PX in the absence of PtdIns(4)P (*i.e.* POPC/POPE (80:20)), but showed a significant increase in penetration when PtdIns(4)P was present in the monolayer (*i.e.* POPC/POPE/PtdIns(4)P (77:20:3)). Thus, as is the case with other PIs, PtdIns(4)P promotes the membrane penetration of its effector proteins, allowing them to penetrate densely packed bilayers, including cell membranes. However, the Bem1p PX domain has higher membrane penetrating activity than other PtdIns(4)P-binding domains in both the absence and presence of PtdIns(4)P.

To elucidate the structural determinant of the high membrane penetrating activity of the Bem1p PX domain, we measured the monolayer penetration of Bem1p PX domain mutants. As shown in Fig. 5*A*, R369A with abrogated PtdIns(4)P binding had significantly lower penetration into the POPC/POPE/PtdIns(4)P (77:20:3) monolayer compared with wild-type Bem1p-PX; it penetrated the POPC/POPE/

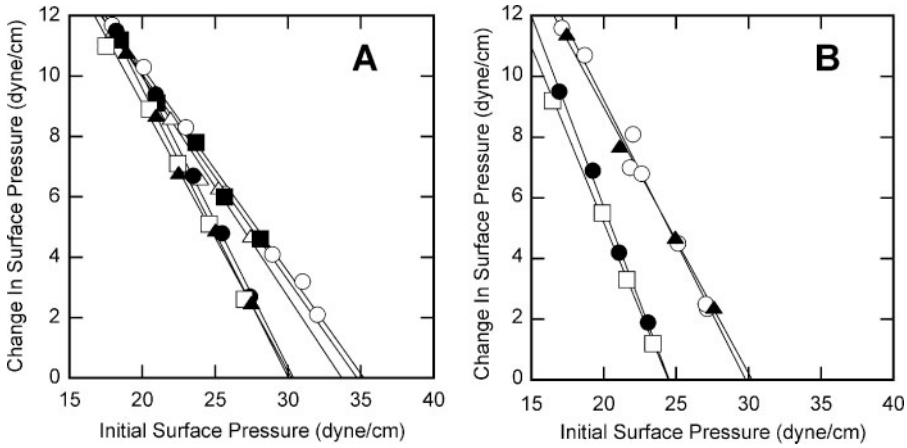

FIGURE 5. **Monolayer penetration of Bem1p mutants.** *A*, $\Delta\pi$ was measured as a function of π_0 for wild-type Bem1p (○), K338A (△), W346A (●), R349A (■), Y360A (□), and R369A (▲) with POPC/POPE/PtdIns(4)P (77:20:3) monolayers. *B*, $\Delta\pi$ was measured as a function of π_0 for wild-type Bem1p (○), W346A (●), Y360A (□), and R369A (▲) with POPC/POPE (80:20) monolayers. The subphase consisted of 10 mM HEPES (pH 7.4) containing 0.16 M KCl. $n = 2$.

PtdIns(4)P (77:20:3) monolayer only as well as the wild type penetrated the POPC/POPE (80:20) monolayer. This verifies the notion that PtdIns(4)P binding to its pocket in Bem1p-PX specifically enhances the monolayer penetration of Bem1p-PX. In contrast, K338A and R349A behaved similarly to the wild type. Furthermore, W346A and Y360A had greatly reduced penetration into both POPC/POPE (80:20) (Fig. 5*B*) and POPC/POPE/PtdIns(4)P (77:20:3) (Fig. 5*A*) monolayers, indicating that these residues are directly involved in the monolayer penetration of the Bem1p PX domain.

It may seem contradictory that Bem1p-PX was able to penetrate the POPC/POPE (80:20) monolayer with surface pressure up to 30 dynes/cm yet showed very low ($\gg$10 mM) affinity for POPC/POPE (80:20) and POPC/POPE/POPS (60:20:20) vesicles in SPR measurements. It should be noted, however, that the surface pressure of large (*i.e.* 100-nm diameter) unilamellar vesicles is estimated to be >30 dynes/cm (83–85). Therefore, despite its relatively high intrinsic membrane penetrating power, Bem1p-PX still cannot effectively bind to and penetrate large vesicles used in SPR studies without PtdIns(4)P-mediated penetration.

Electrostatic Potential Calculations—To account for the unique membrane binding properties of the Bem1p PX domain, we calculated the electrostatic potentials of the domain in the absence and presence of bound PtdIns(4)P. The results are illustrated in Fig. 6. In the absence of PtdIns(4)P and PS, the PI-binding pocket and the cationic patch have a strong positive electrostatic potential due to the presence of multiple cationic residues. This strong positive potential is similar to that seen for other PX domains, including $p40^{phox}$-PX and $p47^{phox}$-PX (78), which was shown to contribute to the initial nonspecific absorption of the domains to the anionic membranes. Likewise, the positive electrostatic potential should drive the initial membrane adsorption of Bem1p-PX, which would then facilitate the specific PtdIns(4)P binding by the domain through lateral diffusion on the membrane surface. Interestingly, the side chain of Tyr^{360} in the PP_{II}-α2 loop near the PI-binding pocket protrudes from the positive electrostatic potential surface. This is an unusual finding because most hydrophobic side chains on the membrane-binding surfaces of PI-binding proteins have been found buried in the positive electrostatic potential in the absence of their cognate PI molecules (7). This unique structural feature explains how Bem1p-PX penetrates the membrane in the absence of PtdIns(4)P. When PtdIns(4)P binds to the domain, the positive electrostatic potential surrounding the membrane-binding surface is greatly reduced, which exposes another hydrophobic residue (Trp^{346}) and facilitates its further membrane insertion, accounting for the enhanced monolayer penetration in the presence of PtdIns(4)P. Fig. 6 also shows that the effect of PS on the electrostatic potential is not significant, which is consistent with the fact that PS and phosphatidic acid do not influence the monolayer penetration of the Bem1p PX domain, although they increase the affinity of Bem1p-PX for PtdIns(4)P-containing membranes.

DISCUSSION

As part of our continuing effort to understand the structural basis of the variable PI specificity of PX domains, we determined the crystal structure of the PtdIns(4)P-binding Bem1p PX domain and characterized its membrane binding properties in this study. High resolution structures of a number of PX domains that bind PtdIns(3)P, PtdIns(3,4)P_2, or PtdIns(4,5)P_2 have been determined as either free proteins or complexes with PIs (46,47,51–55,77). However, no structural information on PtdIns(4)P-binding PX domains has been reported. This study provides new insight into not only the origin of stereospecific PtdIns(4)P recognition by Bem1p-PX, but also the mechanism by which this PX domain interacts with membranes and thereby mediates the function of Bem1p in establishing a new bud in *S. cerevisiae*.

A recently determined crystal structure of the PI3K-C2α PX domain (46) that specifically binds PtdIns(4,5)P_2 revealed why the PX domain does not bind PtdIns(3)P, which most PX domains prefer. In PI3K-C2α-PX, a canonical D3-phosphate ligand (*i.e.* Arg^{58} in $p40^{phox}$-PX) is substituted with Thr, and an acidic residue (Asp^{146}) replaces a D1-phosphate ligand (*i.e.* Arg^{60} in $p40^{phox}$-PX). Similarly, in Bem1p-PX, the consensus D3-phosphate ligand is substituted with Tyr^{317}, and the D1-phosphate ligand is replaced by a buried residue (Pro^{357}). As is the case with PI3K-C2α-PX, these substitutions would not allow PtdIns(3)P to favorably interact with the PI-binding pocket of Bem1p-PX. Other specific structural features of the PI-binding pocket of Bem1p-PX would also prevent productive interaction with all PIs but PtdIns(4)P. Collectively, this negative selection confers high PtdIns(4)P specificity on Bem1p-PX. The difficulty encountered in co-crystallization of Bem1p-PX with its PtdIns(4)P ligand hampered our effort to directly determine the positive structural selection through which the

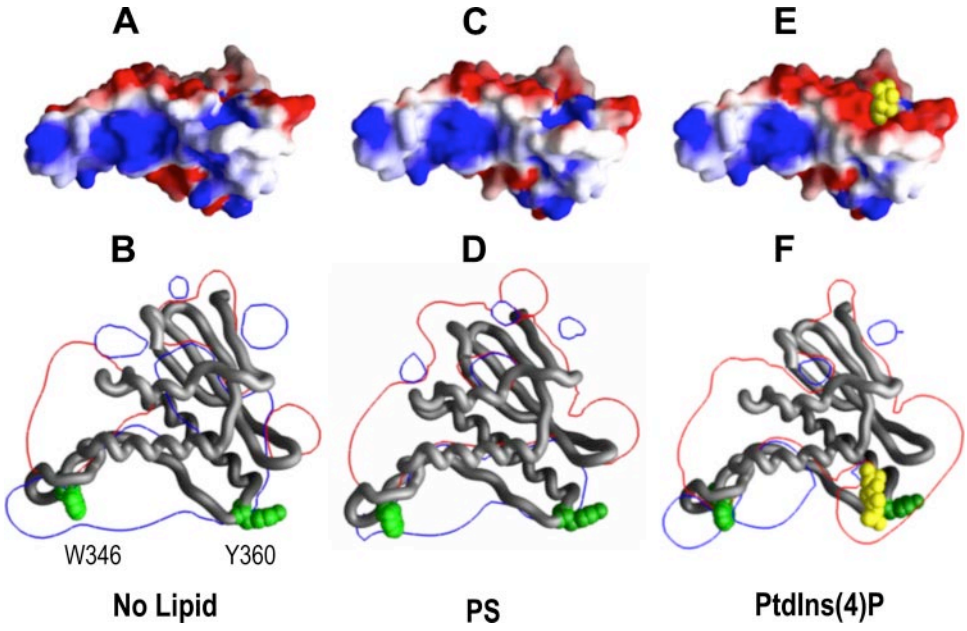

FIGURE 6. **Bem1p PX domain in the absence and presence of PS and PtdIns(4)P.** *A*, *C*, and *E* show the electrostatic potential mapped to the membrane-binding surface of the PX domain. *B*, *D*, and *F* represent the PX domain as a C-α backbone and the electrostatic potential as a two-dimensional contour. The molecules are rotated 90° forward from *A*, *C*, and *E*, and the membrane-binding surfaces point downward in this orientation. Even in the absence of lipids (*A* and *B*), Tyr^{360} is exposed over the electrostatic potential surface, accounting for the high intrinsic membrane penetrating activity of Bem1p-PX. Upon binding to PS (*C* and *D*), the electrostatic potential of the membrane-binding surface of Bem1p-PX is relatively unchanged. Upon binding to PtdIns(4)P (*E* and *F*), the positive electrostatic potential of the membrane-binding surface of Bem1p-PX is greatly decreased, exposing Trp^{346}, which will further penetrate into the membrane. PtdIns(4)P is colored *yellow*, and Trp^{346} and Tyr^{360} are colored *green*. PS is not shown.

domain achieves stereospecific recognition of the D4-phosphate of PtdIns(4)P. However, sequence alignment, modeling, and our mutational analysis strongly suggest that Arg^{369} in Bem1p-PX directly interacts with the D4-phosphate, whereas Lys^{297} is involved in binding to the D1-phosphate.

PX domains have a varying number of cationic residues on their membrane-binding surfaces that promote their nonspecific electrostatic interactions with anionic membranes. For $p47^{phox}$-PX (47) and PLD1-PX (49), some of these cationic residues have been proposed to form secondary lipid-binding pockets on the membrane-binding surface that are separate from the primary PI-binding pockets. The crystal structure of Bem1p-PX suggests that the cationic residues Lys^{338} and Arg^{349} may also form a lipid pocket. However, membrane binding measurements of the wild type and mutants show that this potential pocket is too shallow to accommodate a polar head group and that, consequently, Lys^{338} and Arg^{349} interact nonspecifically with anionic membrane surfaces.

Our previous studies on the FYVE (68, 86), PX (46, 78), and ENTH (81) domains indicated that PI binding specifically induces the membrane penetration of surface hydrophobic/aromatic residues surrounding the PI-binding pocket, presumably by causing local conformational changes in proteins and/or by attenuating the positive electrostatic potential surrounding hydrophobic residues. The crystal structure of Bem1p-PX shows the presence of two prominent aromatic residues, Tyr^{360} and Trp^{346}, located in the PP_{II}-α2 loop and the α1-PP_{II} loop, respectively. Our monolayer and SPR measurements indicated that PtdIns(4)P binding specifically (*i.e.* not induced by other PIs) enhances the membrane penetration of Bem1p-PX. Bem1p-PX also has unusually high PtdIns(4)P-independent monolayer penetrating power, with $\pi_c \approx$ 30 dynes/cm. Our mutational analysis showed that Tyr^{360} and Trp^{346} are largely responsible for the membrane penetrating activity of Bem1p-PX both in the presence and absence of PtdIns(4)P. Our electrostatic calculation suggests that the PtdIns(4)P-independent membrane penetration depends more on Tyr^{360}, whereas the PtdIns(4)P-dependent penetration may involve both Tyr^{360} and Trp^{346}. This is because Tyr^{360} in Bem1p-PX is not embedded in a positive electrostatic potential contour and, consequently, can readily penetrate the membrane without having to pay the hefty desolvation penalty (7, 87) and because PtdIns(4)P binding attenuates the positive electrostatic potential surrounding Trp^{346} in a favorable way.

The electrostatic attenuation of Bem1p-PX caused by PtdIns(4)P binding is, however, less dramatic than that seen with other PX domains (78) and other PI-binding domains (7). Thus, it is also possible that PtdIns(4)P binding promotes the membrane penetration of both Tyr^{360} and Trp^{346} by inducing local conformational changes in the PP_{II}-α2 and α1-PP_{II} loops, perhaps positioning these side chains for better partitioning into the lipid bilayer (7). In this regard, it should be noted that the model of PtdIns(4)P bound to the PI pocket of Bem1p-PX (Fig. 2) assumes a very different orientation from that of PtdIns(3)P in $p40^{phox}$-PX (51) and Vam7p-PX (54, 55), which in turn suggests that Bem1p-PX may dock with lipid membrane surfaces at an angle different from that proposed for $p40^{phox}$-PX (88). For the proposed bound orientation of PtdIns(4)P in the lipid-binding site of Bem1p-PX to occur, the PX domain would need to rotate by ~40° relative to $p40^{phox}$-PX on approach to the membrane surface. It is thus tempting to propose that PtdIns(4)P binding accompanies this molecular motion that juxtaposes the PP_{II}-α2 and α1-PP_{II} loops to the membrane and allows for optimal membrane penetration by Tyr^{360} and Trp^{346}. Undoubtedly, additional studies are necessary to determine exactly how Bem1p-PX docks with PtdIns(4)P-containing membranes.

On the basis of these data, we propose a membrane-binding mechanism for Bem1p-PX. As is the case with other PI-binding domains, Bem1p-PX has a strong positive electrostatic potential due to the presence of basic residues in the PI-binding pocket and on the membrane-binding surface. This positive electrostatic potential should drive the initial adsorption of the domain to anionic membranes and allow its lateral search for PtdIns(4)P on the membrane (7). Although Bem1p-PX has

unusually high PI-independent monolayer penetrating activity, this activity may not be sufficient to drive its binding to compactly packed membranes under normal conditions, judging from the low affinity of Bem1p-PX for POPC/POPE (80:20) and POPC/POPE/POPS (60:20:20) vesicles. Subsequent PtdIns(4)P binding at the membrane surface enhances the membrane penetration of Bem1p-PX and would allow for elongated membrane residence of the domain, which may be important for the physiological function of full-length Bem1p. The high intrinsic membrane penetrating activity of Bem1p-PX may also allow the domain to interact favorably with the local cell membrane with lower surface packing density prior to PtdIns(4)P binding. This type of interaction may be particularly important for keeping the protein on the membrane even after the local depletion of PtdIns(4)P.

It has been shown that Bem1p localizes to the plasma membrane and serves as an adaptor protein that links Cdc24p to other proteins during yeast budding and mating (35, 36). PS is rich in the inner leaflets of most plasma membranes. Also, the presence of PtdIns(4)P has been noted in the yeast plasma membrane (27). The affinity of Bem1p-PX for PtdIns(4)P- and PS-containing membranes is comparable with that of other PtdIns(4)P-binding PH domains under the same conditions. Thus, the interaction of the Bem1p PX domain with the PtdIns(4)P- and PS-containing yeast plasma membrane should promote the specific plasma membrane recruitment of the full-length Bem1p molecules. Protein-protein interactions at the membrane, in addition to PtdIns(4)P-mediated membrane binding of the PX domain, are also expected to contribute to the membrane localization of Bem1p. Bem1p forms complexes with several other proteins, some of which harbor PH domains (33), at sites of budding. Thus, interactions with other membrane-associated proteins could facilitate the assembly of a protein complex at the membrane, as seen with many signaling complexes at the membrane (3).

In summary, this study elucidates the structural basis of the specific PtdIns(4)P binding by the Bem1p PX domain and the mechanism by which this PX domain interacts with PtdIns(4)P-containing membranes. This, in conjunction with our previous work on other PX domains, shows that these small domains with similar molecular architecture achieve diverse PI specificity and distinct membrane binding properties through minor variation of non-conserved residues. This work thus contributes to our understanding of the structure and function of a large family of PX domains that serve as membrane and protein interaction modules during cell signaling and membrane trafficking. This study may also provide the basis of further systematic studies on the membrane recruitment and regulation of Bem1p.

Acknowledgments—The OSBP plasmid was kindly provided by Tim Levine. We thank Olga Perisic for assistance with the structural work and for critically reviewing the manuscript.

REFERENCES

1. Di Paolo, G., and De Camilli, P. (2006) *Nature* **443,** 651–657
2. Roth, M. G. (2004) *Physiol. Rev.* **84,** 699–730
3. Cho, W. (2006) *Sci. STKE* **2006,** PE7
4. Teruel, M. N., and Meyer, T. (2000) *Cell* **103,** 181–184
5. Cremona, O., and De Camilli, P. (2001) *J. Cell Sci.* **114,** 1041–1052
6. Czech, M. P. (2003) *Annu. Rev. Physiol.* **65,** 791–815
7. Cho, W., and Stahelin, R. V. (2005) *Annu. Rev. Biophys. Biomol. Struct.* **34,** 119–151
8. DiNitto, J. P., Cronin, T. C., and Lambright, D. G. (2003) *Sci. STKE* **2003,** RE16
9. Lemmon, M. A., and Ferguson, K. M. (2000) *Biochem. J.* **350,** 1–18
10. DiNitto, J. P., and Lambright, D. G. (2006) *Biochim. Biophys. Acta* **1761,** 850–867
11. Stenmark, H., Aasland, R., and Driscoll, P. C. (2002) *FEBS Lett.* **513,** 77–84
12. Kutateladze, T. G. (2006) *Biochim. Biophys. Acta* **1761,** 868–877
13. Wishart, M. J., Taylor, G. S., and Dixon, J. E. (2001) *Cell* **105,** 817–820
14. Seet, L. F., and Hong, W. (2006) *Biochim. Biophys. Acta* **1761,** 878–896
15. De Camilli, P., Chen, H., Hyman, J., Panepucci, E., Bateman, A., and Brunger, A. T. (2002) *FEBS Lett.* **513,** 11–18
16. Itoh, T., and Takenawa, T. (2002) *Cell. Signal.* **14,** 733–743
17. Itoh, T., and De Camilli, P. (2006) *Biochim. Biophys. Acta* **1761,** 897–912
18. Peter, B. J., Kent, H. M., Mills, I. G., Vallis, Y., Butler, P. J., Evans, P. R., and McMahon, H. T. (2004) *Science* **303,** 495–499
19. Habermann, B. (2004) *EMBO Rep.* **5,** 250–255
20. Dawson, J. C., Legg, J. A., and Machesky, L. M. (2006) *Trends Cell Biol.* **16,** 493–498
21. Bretscher, A., Edwards, K., and Fehon, R. G. (2002) *Nat. Rev. Mol. Cell Biol.* **3,** 586–599
22. Carroll, K., Gomez, C., and Shapiro, L. (2004) *Nat. Rev. Mol. Cell Biol.* **5,** 55–63
23. Cho, W. (2001) *J. Biol. Chem.* **276,** 32407–32410
24. Nalefski, E. A., and Falke, J. J. (1996) *Protein Sci.* **5,** 2375–2390
25. Rizo, J., and Sudhof, T. C. (1998) *J. Biol. Chem.* **273,** 15879–15882
26. Cho, W., and Stahelin, R. V. (2006) *Biochim. Biophys. Acta* **1761,** 838–849
27. Wera, S., Bergsma, J. C., and Thevelein, J. M. (2001) *FEMS Yeast Res.* **1,** 9–13
28. Chant, J., and Pringle, J. R. (1995) *J. Cell Biol.* **129,** 751–765
29. Zahner, J. E., Harkins, H. A., and Pringle, J. R. (1996) *Mol. Cell. Biol.* **16,** 1857–1870
30. Adams, A. E., Johnson, D. I., Longnecker, R. M., Sloat, B. F., and Pringle, J. R. (1990) *J. Cell Biol.* **111,** 131–142
31. Bender, A., and Pringle, J. R. (1991) *Mol. Cell. Biol.* **11,** 1295–1305
32. Hartwell, L. H. (1971) *Exp. Cell Res.* **69,** 265–276
33. Bose, I., Irazoqui, J. E., Moskow, J. J., Bardes, E. S., Zyla, T. R., and Lew, D. J. (2001) *J. Biol. Chem.* **276,** 7176–7186
34. Irazoqui, J. E., Gladfelter, A. S., and Lew, D. J. (2003) *Nat. Cell Biol.* **5,** 1062–1070
35. Ito, T., Matsui, Y., Ago, T., Ota, K., and Sumimoto, H. (2001) *EMBO J.* **20,** 3938–3946
36. Shimada, Y., Gulli, M. P., and Peter, M. (2000) *Nat. Cell Biol.* **2,** 117–124
37. Ago, T., Takeya, R., Hiroaki, H., Kuribayashi, F., Ito, T., Kohda, D., and Sumimoto, H. (2001) *Biochem. Biophys. Res. Commun.* **287,** 733–738
38. Vollert, C. S., and Uetz, P. (2004) *Mol. Cell. Proteomics* **3,** 1053–1064
39. Ponting, C. P. (1996) *Protein Sci.* **5,** 2353–2357
40. Kanai, F., Liu, H., Field, S. J., Akbary, H., Matsuo, T., Brown, G. E., Cantley, L. C., and Yaffe, M. B. (2001) *Nat. Cell Biol.* **3,** 675–678
41. Cheever, M. L., Sato, T. K., de Beer, T., Kutateladze, T. G., Emr, S. D., and Overduin, M. (2001) *Nat. Cell Biol.* **3,** 613–618
42. Ellson, C. D., Gobert-Gosse, S., Anderson, K. E., Davidson, K., Erdjument-Bromage, H., Tempst, P., Thuring, J. W., Cooper, M. A., Lim, Z. Y., Holmes, A. B., Gaffney, P. R., Coadwell, J., Chilvers, E. R., Hawkins, P. T., and Stephens, L. R. (2001) *Nat. Cell Biol.* **3,** 679–682
43. Song, X., Xu, W., Zhang, A., Huang, G., Liang, X., Virbasius, J. V., Czech, M. P., and Zhou, G. W. (2001) *Biochemistry* **40,** 8940–8944
44. Xu, Y., Hortsman, H., Seet, L., Wong, S. H., and Hong, W. (2001) *Nat. Cell Biol.* **3,** 658–666
45. Yu, J. W., and Lemmon, M. A. (2001) *J. Biol. Chem.* **276,** 44179–44184
46. Stahelin, R. V., Karathanassis, D., Bruzik, K. S., Waterfield, M. D., Bravo, J., Williams, R. L., and Cho, W. (2006) *J. Biol. Chem.* **281,** 39396–39406
47. Karathanassis, D., Stahelin, R. V., Bravo, J., Perisic, O., Pacold, C. M., Cho, W., and Williams, R. L. (2002) *EMBO J.* **21,** 5057–5068

48. Lee, J. S., Kim, J. H., Jang, I. H., Kim, H. S., Han, J. M., Kazlauskas, A., Yagisawa, H., Suh, P. G., and Ryu, S. H. (2005) *J. Cell Sci.* **118,** 4405–4413
49. Stahelin, R. V., Ananthanarayanan, B., Blatner, N. R., Singh, S., Bruzik, K. S., Murray, D., and Cho, W. (2004) *J. Biol. Chem.* **279,** 54918–54926
50. Cheng, G., and Lambeth, J. D. (2004) *J. Biol. Chem.* **279,** 4737–4742
51. Bravo, J., Karathanassis, D., Pacold, C. M., Pacold, M. E., Ellson, C. D., Anderson, K. E., Butler, P. J., Lavenir, I., Perisic, O., Hawkins, P. T., Stephens, L., and Williams, R. L. (2001) *Mol. Cell* **8,** 829–839
52. Xing, Y., Liu, D., Zhang, R., Joachimiak, A., Songyang, Z., and Xu, W. (2004) *J. Biol. Chem.* **279,** 30662–30669
53. Zhou, C. Z., de La Sierra-Gallay, I. L., Quevillon-Cheruel, S., Collinet, B., Minard, P., Blondeau, K., Henckes, G., Aufrere, R., Leulliot, N., Graille, M., Sorel, I., Savarin, P., de la Torre, F., Poupon, A., Janin, J., and van Tilbeurgh, H. (2003) *J. Biol. Chem.* **278,** 50371–50376
54. Lee, S. A., Kovacs, J., Stahelin, R. V., Cheever, M. L., Setty, T. G., Burd, C., Cho, W., and Kutateladze, T. G. (2006) *J. Biol. Chem.* **281,** 37091–37101
55. Lu, J., Garcia, J., Dulubova, I., Sudhof, T. C., and Rizo, J. (2002) *Biochemistry* **41,** 5956–5962
56. Kates, M. (1986) *Techniques of Lipidology*, 2nd Ed., pp. 114–115, Elsevier Science Publishers B. V., Amsterdam
57. Leslie, A. G. W. (1992) *Joint CCP4 and ESF-EACMB Newsletter on Protein Crystallography*, Daresbury Laboratory, Warrington, UK
58. Collaborative Computational Project (1994) *Acta Crystallogr. Sect. D Biol. Crystallogr.* **50,** 760–763
59. Terwilliger, T. C., and Berendzen, J. (1999) *Acta Crystallogr. Sect. D Biol. Crystallogr.* **55,** 849–861
60. Vonrhein, C., Blanc, E., Roversi, P., and Bricogne, G. (2006) *Methods Mol. Biol.* **364,** 215–230
61. Abrahams, J. P., and Leslie, A. G. (1996) *Acta Crystallogr. Sect. D Biol. Crystallogr.* **52,** 30–42
62. Cowtan, K., and Main, P. (1998) *Acta Crystallogr. Sect. D Biol. Crystallogr.* **54,** 487–493
63. Perrakis, A., Morris, R., and Lamzin, V. S. (1999) *Nat. Struct. Biol.* **6,** 458–463
64. Jones, T. A., Zou, J.-Y., Cowan, S. W., and Kjeldgaard, M. (1991) *Acta Crystallogr. Sect. A* **47,** 110–119
65. Murshudov, G. N., Vagin, A. A., and Dodson, E. J. (1997) *Acta Crystallogr. Sect. D Biol. Crystallogr.* **53,** 240–255
66. Laskowski, R. A., MacArthur, M. W., Moss, D. S., and Thornton, J. M. (1993) *J. Appl. Crystallogr.* **26,** 283–291
67. Ho, S. N., Hunt, H. D., Horton, R. M., Pullen, J. K., and Pease, L. R. (1989) *Gene* (*Amst.*) **77,** 51–59
68. Stahelin, R. V., Long, F., Diraviyam, K., Bruzik, K. S., Murray, D., and Cho, W. (2002) *J. Biol. Chem.* **277,** 26379–26388
69. Bittova, L., Sumandea, M., and Cho, W. (1999) *J. Biol. Chem.* **274,** 9665–9672
70. Bittova, L., Stahelin, R. V., and Cho, W. (2001) *J. Biol. Chem.* **276,** 4218–4226
71. Stahelin, R. V., and Cho, W. (2001) *Biochemistry* **40,** 4672–4678
72. Cho, W., Bittova, L., and Stahelin, R. V. (2001) *Anal. Biochem.* **296,** 153–161
73. Nicholls, A., Sharp, K. A., and Honig, B. (1991) *Proteins* **11,** 281–296
74. Honig, B., and Nicholls, A. (1995) *Science* **268,** 1144–1149
75. Brooks, B. R., Bruccoleri, R. E., Olafson, B. D., States, D. J., Swaminathan, S., and Karplus, M. (1983) *J. Comp. Chem.* **4,** 187–217
76. Sali, A., and Blundell, T. L. (1993) *J. Mol. Biol.* **234,** 779–815
77. Xing, Y., and Xu, W. (2003) *Acta Crystallogr. Sect. D Biol. Crystallogr.* **59,** 1816–1818
78. Stahelin, R. V., Burian, A., Bruzik, K. S., Murray, D., and Cho, W. (2003) *J. Biol. Chem.* **278,** 14469–14479
79. Levine, T. P., and Munro, S. (1998) *Curr. Biol.* **8,** 729–739
80. Levine, T. P., and Munro, S. (2002) *Curr. Biol.* **12,** 695–704
81. Stahelin, R. V., Long, F., Peter, B. J., Murray, D., De Camilli, P., McMahon, H. T., and Cho, W. (2003) *J. Biol. Chem.* **278,** 28993–28999
82. Flesch, F. M., Yu, J. W., Lemmon, M. A., and Burger, K. N. (2005) *Biochem. J.* **389,** 435–441
83. Demel, R. A., Geurts van Kessel, W. S., Zwaal, R. F., Roelofsen, B., and van Deenen, L. L. (1975) *Biochim. Biophys. Acta* **406,** 97–107
84. Blume, A. (1979) *Biochim. Biophys. Acta* **557,** 32–44
85. Marsh, D. (1996) *Biochim. Biophys. Acta* **1286,** 183–223
86. Blatner, N. R., Stahelin, R. V., Diraviyam, K., Hawkins, P. T., Hong, W., Murray, D., and Cho, W. (2004) *J. Biol. Chem.* **279,** 53818–53827
87. Murray, D., and Honig, B. (2002) *Mol. Cell* **9,** 145–154
88. Malkova, S., Stahelin, R. V., Pingali, S. V., Cho, W., and Schlossman, M. L. (2006) *Biochemistry* **45,** 13566–13575
89. Engh, R. A., and Huber, R. (1991) *Acta Crystallogr. Sect. A* **47,** 392–400